THE INFLUENCE OF THE SLM PROCESS PARAMETERS OPTIMIZATION ON THE DENSITY AND MICROSTRUCTURE OF TI6AL4V ALLOY

Anna Woźniak, Marcin Adamiak

Silesian University of Technology, Faculty of Mechanical Engineering, Department of Engineering Materials and Biomaterials, Konarskiego 18A, 44-100 Gliwice, Poland

Corresponding author: Anna Woźniak, anna.wozniak@polsl.pl

Abstract: The Selective Laser Melting/Selective Laser Sintering SLM/SLS is one of the most popular of the additive manufacturing AM method that allows the layer-wise production of parts in metallic materials. The bed fusion method methods don't appear limitation for the design point view, but the properties of the final elements depend on the process parameters. The study presents the results of density measurements, microscopic observation and chemical and phase compositions analysis. Based on the obtained results it can be concluded that the most important parameters, which have a significant effect on the properties of the SLM/SLS part was laser power and scanning speed. The elements produced using the optimum parameter were characterized by 99 % density comparable to the value in the material card.
Key words: SLM/SLS, parameters optimization, Ti6Al4V, μCT, SEM/EDS analysis.

1. INTRODUCTION

The Ti6Al4V alloy is one of the most popular metal biomaterials in various medical applications, including dental and orthopedic implants, fracture fixation or elements of heart valves, owing to it's the better corrosion resistance, more favorable mechanical properties, relatively low elastic modulus, low specific weight, and acceptable biocompatibility compared with other traditional metallic biomaterials, such as stainless steel and cobalt based alloy. Among these materials, Ti and its alloys are widely used for long-term, load-bearing implants [1-6]. The titanium based alloys are usually begging processed by conventional manufacturing methods such as casting, solidification or powder metallurgy. However, the high reactivity of titanium and its high affinity to the oxygen are some of the typical challenges for traditional processed methods. Currently, based on the literature data, it can be stated increase of useage of additive manufacturing methods, such as Selective Laser Sintering/Selective Laser Melting SLS/SLM techniques. Additive Manufacturing AM techniques can be easily applied to producing the complex parts, giving properties equivalent or superior to the one obtained by conventional routes [6-12]. The final SLM elements are characterized also by good dimensional accuracy. During the SLS/SLM procedure the powder material is spread across the build platform using a blade or counter-rotating powder leveling roller. The layer thickness of the powder is typically in the range between 10 and 100 μm. In the next steps the laser exposition is started. The laser beam is moving according to the designed bitmap, scans and melts the powder material. Each layer of the element is filled with elongated tracks of melted powder [12-16]. As the heating laser beam moves away, the molten pool as a result of thermal phenomena are cooling down and solidifies with a rate of 10000-100000°C/s and a cross-section of the detail is created. Next, the building platform is lowered to the distance of the layer thickness. All of the stages of the process are returned, until the final elements are full. In order to decrease the degradation and oxidation of metal material, the SLS/SLM processes are conducted in an inert gas atmosphere, such as argon or hydrogen. The properties of final SLS/SLM parts depended by the process parameters optimization – scanning speed SP [mm/s], laser output power P [W], laser beam diameter [μm], point distance PD [μm], hatch distance HD [μm] and layer thickness t [μm]. One of the most frequently detected defects of final elements is porosity and for these reasons the typical process parameters optimization towards minimization of porosity are used. Additionaly, the influence of the process parametres optimization on the microstructures of the Ti6Al4V parts, manufacturing using bed fusion technologies were extensively studied [19, 20].

However, there are serval possibilities for measuring the density of final details, such as analysis of a micrograph of a cross-section of the part and non-destructive methods such as e.g. Archimedes method and X-ray or neutron imaging. However, the most accurate measurement method should be indicated [15-20].

This article aims to determine the impact of SLS/SLM process optimization on the degree

of porosity of Ti6Al4V parts and to characterize the material structure and properties.

2. MATERIALS AND METHODS

The material for the research was Ti6Al4V titanium alloy, which was purchased from Renishaw Company with chemical composition given in Table 1.

Table 1. Chemical composition of Ti6Al4V alloy powder

Element	Al	V	Fe	O	C
Mass (%)	5.50-6.50	3.50-4.50	≤0.25	≤0.13	≤ 0.08
Element	Ni	H	Y	Ti	
Mass (%)	≤0.05	≤0.012	≤0.005	balance	

The powder grains were dominantly regular with spherical in the shape (Figure 1) and the powder particle size was in the range of 20-45 µm, with an average of 30 µm, as measured using a laser particle size analyzer, Analysette 22 MicroTec Plus.
The tested samples were manufactured by the SLM/SLS process, which was performed using Renishaw AM250 rapid manufacturing system (Renishaw) that employs a Ytterbium fiber laser YFL with a wavelength of approximately 1064-1070 nm with average maximum laser output power of 400W, maximum scanning speed up to 2000 mm/s. Laser beam diameter equals to 70 µm. The machine is also equipped with two oxygen sensors to ensure low oxygen content during the process. Reducing the oxygen concentration to about 100 ppm is associated with the need to minimize the process of oxidation and degradation of the used powder material. For this reason, the processes were conducted under the protective atmosphere of high purity argon - the working chamber was flooded with 99.996% pure argon until the value below 0.1% of oxygen was reached. A pure titanium base plate was used for manufacturing the tested samples. Before starting the SLM/SLS process itself, the base plate was polished to guarantee good adhesion of the powder material. Additionally, the plate was heated up to 150°C and was kept at the same level throughout the whole process until the details were complete.

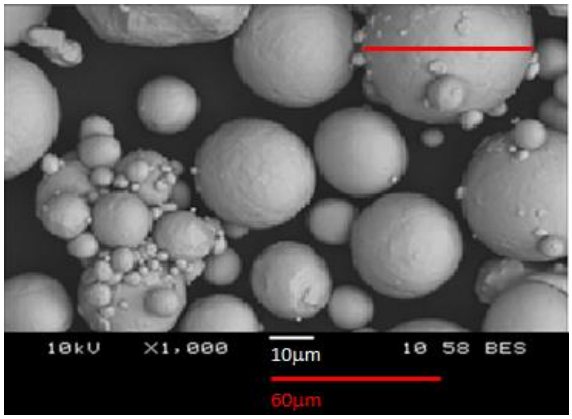

Fig. 1. SEM image of Ti6Al4V powder

In the experimental part the attempt was made to determine the influence of values of SLM/SLS process parameters on the density and properties of final samples. Based on the literature data [11-13], it can be concluded that the most important parameters, which have a significant effect on the quality of the SLM/SLS parts is P and SP. These factors define the linear energy density delivered by a laser beam to the powder material. To obtain by SLM/SLS process a good, full density functional part, the particles of the layer of powder material must receive a satisfactory amount of energy through the laser melting process. The values of P and SP were variable. The layer thickness t and exposure time E_t remained constant throughout the manufacturing process. The tested samples were in the form of a cube, 10x10x10 mm in size. The process parameters were presented in Table 2. A meander scan strategy was employed for the manufacturing of all the tested samples, which were built at 0° to the build direction. The process parameters and the scanning strategy were designed by MARCAM AutoFAB software.

Table 2. The SLM/SLS process parametres

Parameters	Value
P, [W]	300, 350, 400
SP , [mm/s]	100, 300, 500, 700
HD, [µm]	110
PD, [µm]	75
E_t, [µs]	100
t , [µm]	30

The samples subjected to microscopic observation were grinding and polishing. The grinding process was performed using abrasive paper with a grain size of 500, 800, 1200, 2400 and 4000 grain/mm^2 and next the polishing process was carried out with colloidal silica suspension OP-U 0.04 µm. The mechanical treatment was using grinding-polishing machine TERGAMIN-30 (Struers). A Kroll`s reagent – HNO_3: HF: H2O (4:1:1 vol.) was used for samples etching.

2.1 Density measurements

Archimedes methods

For the Archimedes methods, the analytical Radwag balance AS 220.R2 type with the measuring accuracy of ± 0.1 mg was used. The schematic of the measuring principle indicating the measuring of the mass in air and the fluid and are shown in Figure 2. The measurements were performed using of deionized water. Each sample, before density measurements, were placed in an ultrasonic bath for 15 minutes, afterwards samples were measured independently four times. The calculation of the dentistry ρ_p of the SLM/SLS elements under consideration follows equation (1), where ρ_{fl} is the density of the fluid, which was temperature-

dependent (T = 24 ± 1°C), m_a is the mass of the details in air and m_{fi} is the mass of the details in the fluid.

$$\rho_P = \frac{m_a}{m_a - m_{fi}} \cdot \rho_{fi} \quad (1)$$

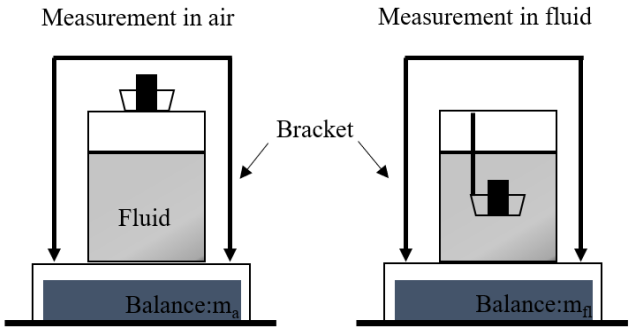

Fig. 2. Schematic of the Archimedes method for density measurement

Microscopic observation

Cross-sections perpendicular – the XY plane and parallel -XZ plane to the build direction (OZ axis), were prepared from the final SLM/SLS samples for surface topography observation, which were carried out using stereomicroscope SteREO Discovery V8 by Zeiss. The specimens were observed without using etching, For each cross-section of the tested samples using three different magnifications, micrographs were taken at random positions. The obtained pictures were analyzed using GIMP software. The correct black content (porosity) of the cross-section can be identified using the inbuilt histogram function.

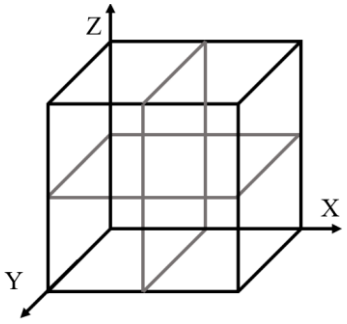

Fig. 3. Geometry of the tested samples with positions of the micro CT samplecut in the YX and XZ planes

MicroCT scanning

The density of the cubic samples was determined to by μCT scanning using a pixel size set of 2.91 μm, and a 360° sample rotation step of 0.3°. The porosity analysis was performed using MyVGL software.

2.2 SEM/EDS analysis

The Scanning Electron Microscope SEM was used for the surface topography and microstructure of the tested samples observations. The microscopic examination was performed using Supra 35 scanning microscope by Zeiss, equipped with secondary electrons SE detector and back-scatter electron detector QBSD. The observations were conducted with an accelerating voltage of 20 kV. Additionally, the qualitative and quantitative of the microchemical composition were performed using the X-ray energy dispersive spectroscopy (EDS) analysis. The SEM/EDS analysis was carried out using a point-by-point method on the surface of the tested samples, and the results of measurements were presented in the form of characteristic X-ray spectra, also the element contents were determined.

2.3 XRD analysis

The phases of tested samples were examined using the X`Pert PRO X-ray diffractometer (Panalytical) with Cu radiation. The using lamp was set to 40 kV and the heater current of 30 mA was used. The XRD phase analysis was carried out according to the Bragg-Brentano geometry, using the PICcel 3D detector. The XRD pattern was obtained employing a scanning step of 0.05. The measurements of each sample were performed withing the 2Θ Bragg angle ranging from 40 to 90°.

3. RESULTS AND DISCUSSIONS

3.1 Density measurements

The results of the density of final parts measurements are predent in Table 3. Exemplary results of macroscopic observations are presented in Figure 4. Additionally, the typical SLS/SLM parts defect are shown in Figure 5. The relative density of the final element is associated with the uncontrolled porosity, which is one of the most frequently observed defects of the SLS/SLM parts and it is an indicator of final quality. Based on the buoyancy method it can be concluded that the density of all tested samples was between 72.6 % and 101.3 %, depending on the processing parameter, and similar results were registered for the second measuring method – from 74.9 % to 101 %. It can be observed that increasing the values of the SP - 500, 700 mm/s and/or decrease the values of P 300 W (Figure 5(c)) lead to decrease the density of the final elements, which is related to insufficient energy to melt and diffuse the powder material. The final build would end with entrapment of the voids among the particles of metal as a result of the incomplete melting. The lack-of fusion pores (Figure 5(a)) are the irregular cavities (irregular-wedge shape or band shape with sharp tips and large dimensional with short axes aligned in the building direction of the SLS/SLM parts), filled by metallic spherical particles. At the low values of SP – 100 mm/s and high values of P – 400 W, the molten pool

overheating occurs, which cause generated other defect of the part such as keyhole formation, because of vaporization, which increases the overall porosity level. Additionally, the shape of the scan tracks can change into two droplets, which is associated with Plateau-Rayleigh instability. The Plateau-Rayleigh instability leads to the formation of irregular voids associated with gas entrapment (Figure 5(c)) or unbelted powder particles (Figure 5(b)). Generally, the gas pores are spherical or elliptical in the shape (with a diameter of about 1-100 μm) and are stochastically distributed in the entire volume of the SLM. These spherical voids formed as a result of trapping of gas (Oxygen, Hydrogen, Argon or Nitrogen) in the lowest parts of the molten pool. The high cooling rate and the temperature gradient along the build direction (OZ axis) lead to impossibility of gas to complete escape. The trapped gas didn`t escape in time and was hence stuck in the melted track. Additionally, at high value of laser power combined with a relatively low scanning speed, the scan track could be completely melted and next broke up duo the excessive shrinkage and the high residual stresses, forming many visible cracks (Figure 5(b)). The higher values value of the material density was obtained for the samples, manufacturing using a high value of laser power (P = 400 W) and middle value of scanning speed (SP = 500mm/s), which the mean value was an approximately $\rho = 4.4 \pm 0.01$ g/cm^3 both measuring methods, what constitutes an approximately 99.5% of the theoretical value ($\rho = 4.42$ g/cm^3). The μ-CT results for this samples group are shown in Figure 6. The calculated porosity based on μ-CT reconstructions of the samples was 0.1%.

Table 3. Results of the density measurements

P, [W]	SP, [mm/s]	Density, [g/cm^3] Archimedes method	Micographs analysis
300	100	3.72 ± 0.13	3.78 ± 0.15
350		4.14 ± 0.04	4.25 ± 0.10
400		4.18 ± 0.10	4.12 ± 0.11
300	300	3.55 ± 0.10	3.60 ± 0.14
350		4.30 ± 0.05	4.37 ± 0.08
400		4.34 ± 0.01	4.40 ± 0.01
300	500	3.40 ± 0.10	3.45 ± 0.12
350		4.22 ± 0.03	4.25 ± 0.05
400		4.38 ± 0.02	4.35 ± 0.05
300	700	3.21 ± 0.09	3.21 ± 0.10
350		4.12 ± 0.03	4.20 ± 0.08
400		4.20 ± 0.02	3.32 ± 0.03

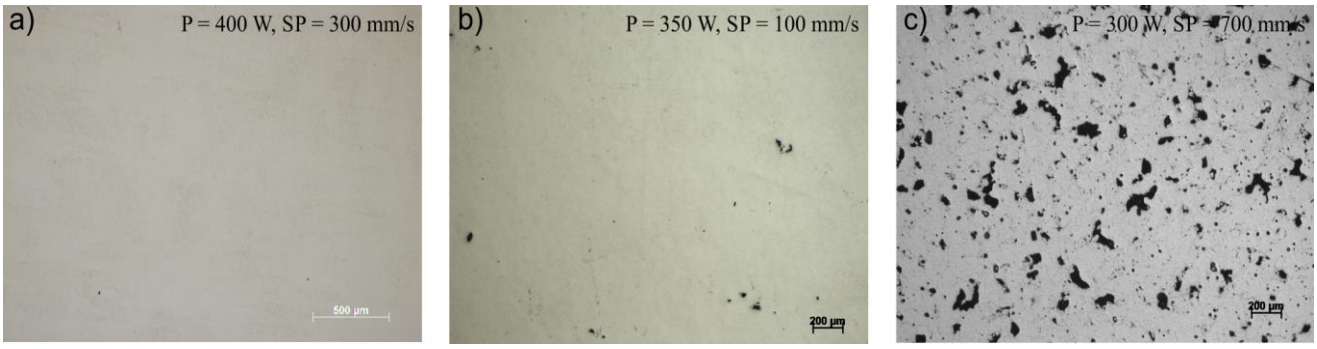

Fig. 4. Example results of microscopic observation, LM

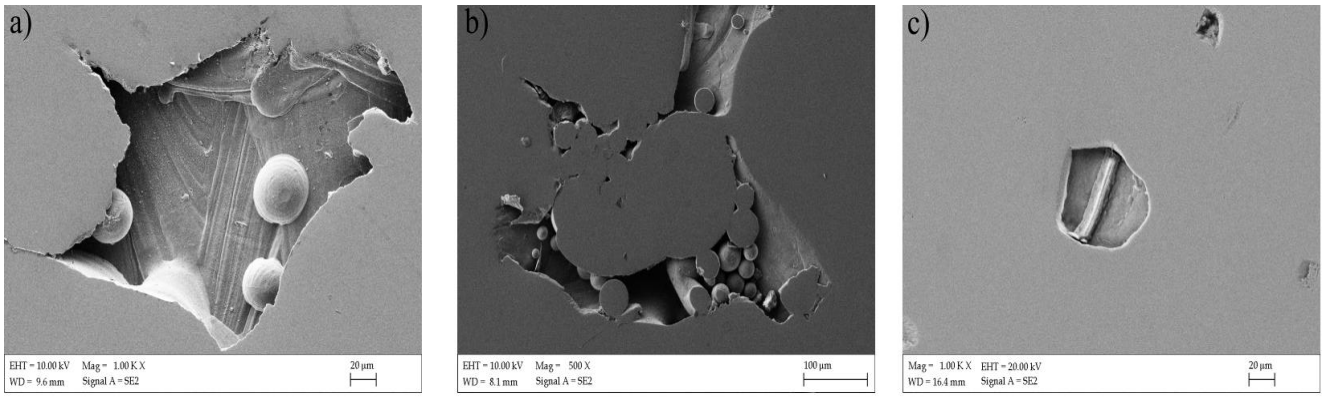

Fig. 5. Example results of microscopic observation SEM, a) lack-of-fusion pores, b) binding effect, c) gas pore

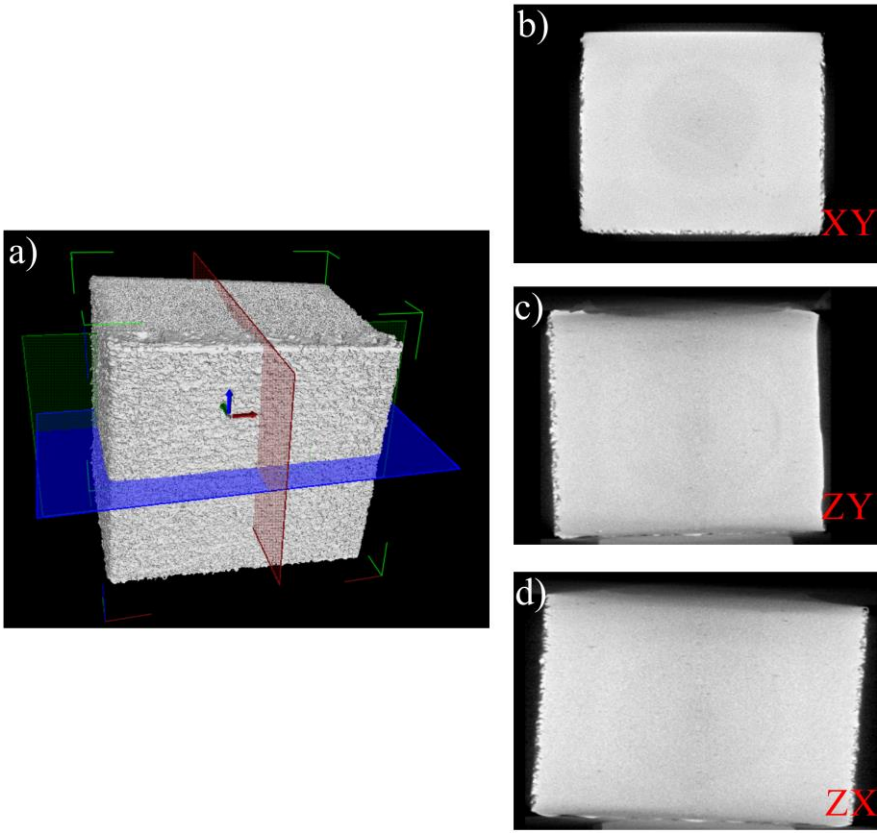

Fig. 6. Results of microtogaphy analysis, μCT

Additionally, based on the obtained results, it can be consulted that the standard deviation is increasing to even 0.13 g/cm^3 for the lower densities, which can be associated more incomplete melting of the powder particles at a lower value of the P and higher value of SP. Additionally, the higher values of the standard deviations were obtained for the measurements obtained for the micrographs analysis. Based on this it can be concluded that the Archimedes method delivers more reliable results, because of the whole sample volume is taken into account instead of some single cross-sections, which might not represent a typical porosity of the sample.

Based on the obtained results of density measurements and a processing map (Figure 7) was then defined. Over the entire range of P and SP, three processing windows could be summarized, corresponding to three different melting mechanisms:

I. Melting with the cracks or porosity in the effect of the vaporization – generally, At the high values of the P and relatively low values of the SP, the powder material of Ti6Al4V alloy could be completely melted, but the single tracks in the effect of high residual stresses and excessive shrinkage could be broke up, forming many visible cracks. Additionally, as a result of molten pool overheating, the vaporization process can provide to defects of the manufactured parts.

II. Melting – the combination of high values of the P (400 W) and intermediate values of the SP (300, 500 mm/s), guarantee stable tracks during laser exposition. Parts manufactured using these parameters have a density of 98% relative to the reference value.

III. Partial melting – a combination of the low values of the P and high values of SP could be insufficient for significant melting of the SLS/SLM parts. The final elements are characterized by very low density.

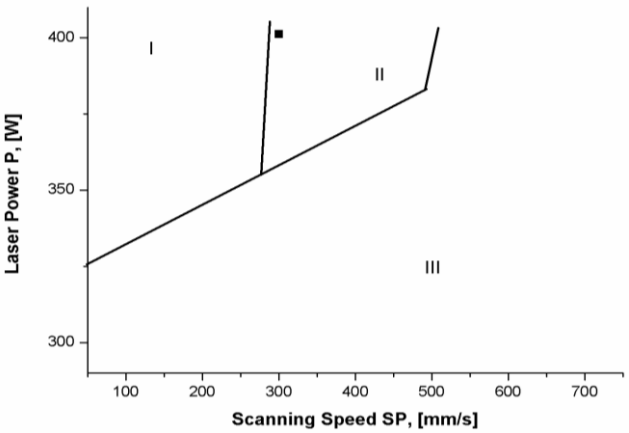

Fig. 7. Windows of parametres for the Ti6Al4V components manufactured by SLM/SLS process; I - melting with the cracks or porosity, II – full melting, III - partial melting

The highest values of the density of tested samples were obtained using a combination of P = 400 W and SP = 500 mm/s, and the mean value was an

approximately ρ = 4.38 ± 0.02 g/cm^3 (Archimedes method) and ρ = 4.35 ± 0.05 g/cm^3 (Micrographs analysis). Additionally, the μ-Ct analysis suggests that the level of the porosity of this samples group was 0.1 %.

Based on the results of density measurements, significant differences in the results obtained from different measure methods. The repeatability of the Archimedes method is higher than for the microscopic analysis and this is most visible especially for low-density elements. The micrograph analysis technique is a destructive method, requiring proper preparation of cross-sections of elements. Besides, computer analysis may not be reliable due to the quality of microscopic images and possible shadows. In this case, the most important role is played by the accuracy of the mechanic treatment of the samples. Additionally, the Archimedes method is the most economic and fast procedure of density measurements compared to the other methods. Taking into account the laws of the physics and buoyancy of the details in the liquid (deionized water), obtained results are very reliable. The micrographs analysis may prove useful to get information of the size and shape of the pores. The μ-Ct can be beneficial to confirm the density of elements and the resulting analysis of cross-sections of the final element. Besides, CT analysis can provide relevant information in the presence of clogged porosity.

3.2 Microstructure analysis

The results of SEM/EDS analysis and the results of X-ray diffraction qualitative phase analysis of tested samples are shown in Figures 8-10. It is observed that for the tested samples, most of the peaks have a hexagonal close-packed hcp Ti structure, which can be attributed to either α-Ti phase or α`-Ti martensite phase since both phases have the same crystalline structure and similar lattice parameters. Because of similarity between the α phase and the α′ phase, it is difficult to differentiate the two phases [21-25]. Formation of hexagonal martensite occurs due to high cooling rates from β field temperatures involved in the process, which are sufficient to induce martensitic transformation.

However, when heated, the α-Ti phase is nucleated along the martensite α` boundaries and vanadium atoms are expelled leading to the formation of β at α phase boundaries. For this reason, as a result of heat treatment the long α` needles can be transformed into the long and thick α lamellar. The SEM image presented in Figures 9 and 10 show that the phases are mainly α-Ti, and hence the hcp structure shown in the XRD pattern can be attributed to α-Ti, not α`-Ti phase. Based on this it can be concluded, that the tested samples present a finely distributed α phase and a relatively smaller percentage of β phase, such as a commercial Ti6Al4V alloy used for biomedical applications [26, 27]. Additionally, the SEM/EDS analysis pointed to the increased concentration of vanadium V for the β phase, and increase of aluminium Al for α phase.

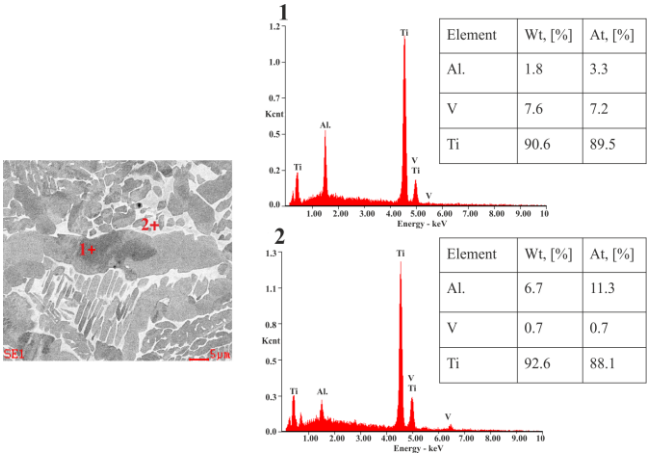

Element	Wt, [%]	At, [%]
Al.	1.8	3.3
V	7.6	7.2
Ti	90.6	89.5

Element	Wt, [%]	At, [%]
Al.	6.7	11.3
V	0.7	0.7
Ti	92.6	88.1

Fig. 8. The SEM/EDS analysis

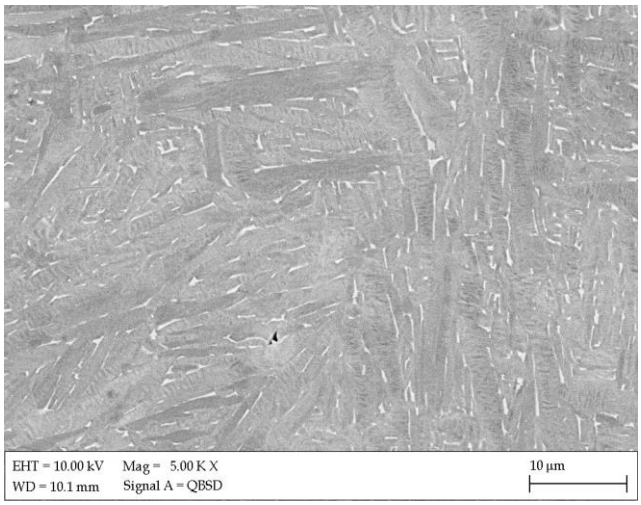

Fig. 9. The Microstructure of Ti6Al4V alloy, SEM

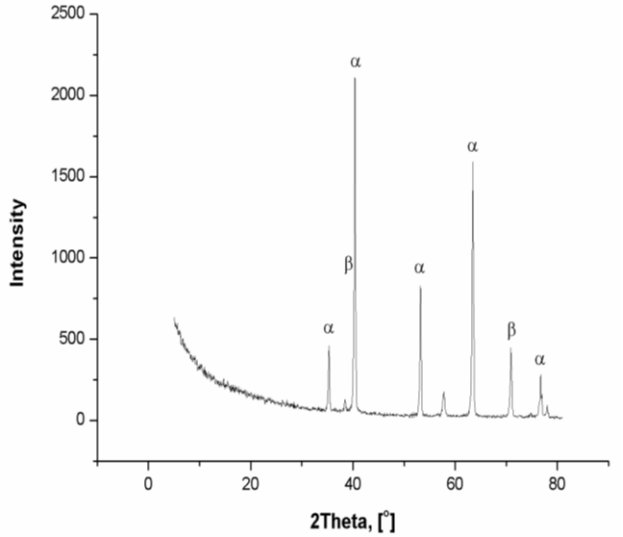

Fig. 10. X-ray diffraction pattern of investigated alloy

4. CONCLUSIONS

Based on the obtained results it can be concluded:
-The final quality of the tested samples and their properties, densification level and microstructure of SLS/SLM parts depend strongly on the two main process parameters – laser power and scanning speed, which have the significant effect on the operating temperature of the melting system.
-The higher value of material density was obtained for the samples, manufactured using high value of P = 400 W and low valye of SP = 500 mm/s - $\rho = 4.38 \pm 0.02$ g/cm^3 (Archimedes method) and $\rho = 4.35 \pm 0.05$ g/cm^3 (Micrographs analysis).
-Combination of high P and low SP, results to the single tracks cracking; meanwhile, low value of P and high value of SP lead to incomplete melting.
-Microstructure of the tested samples consists of a finely distributed α phase and a relatively smaller percentage of β phase.

5. REFERENCES

1. I. Światkowska, J.F.W. Mosselmans, T. Geraki, C.C. Wyles, J.J. Maleszeski, J. Henckel, B. Sampson, D.B. Potter, I. Osman, R.T. Trousdale, A.J. Hart, (2018). *Synchrotron analysis of human organ tissue exposed to implant material*, Journal of Trace Elemements in Medicine and Biology, **46**, 128–137.
2. Q. Chen, G. A. Thouas, (2015). *Metallic implant biomaterials*, Materials Science and Engineering: R Reports, **87**, 1–57.
3. M. F. F. A. Hamidi, W.S.W. Harun, M. Samykano, S.A.C. Ghani, Z. Ghazalli, F. Ahmad, A.B. Sulong, (2017). *A review of biocompatible metal injection moulding process parameters for biomedical applications*, Materials Scinece and Engineering: C, **78**, 1263–1276.
4. M. Basiaga, W. Kajzer, W. Walke, A. Kajzer, M. Kaczmarek, (2016). *Evaluation of physicochemical properties of surface modified Ti6Al4V and Ti6Al7Nb alloys used for orthopedic implants*, Materials. Science Engineering: C, **68**, 851–860.
5. A. Woźniak, B. Ziębowicz, A. Ziębowicz, W. Walke. (2018). *Physicochemical properties of oxide ZrO2 layer deposited by sol-gel metgod on Ti-6Al-4V allot*, Archives of Metallurgy and Materials, **63**(3), 1209-1215.
6. A. Ziębowicz A, A. Woźniak, B. Ziębowicz B, K. Kosiel, G. Chladek, (2018). *The effect of atomic deposition of ZrO_2 on the physicochemical properties of cobalt based alloys intended for prothetic dentistry*, Archives of Metallurgy and Materials, **63**(3), 1077-1082.
7. A. Masmoudi, R. Bolot, and C. Coddet, (2015). *Investigation of the laser–powder–atmosphere interaction zone during the selective laser melting process*, Journal of Materials Processing Technology, **225**, 122–132.
8. A. G. Demir and B. Previtali, (2017). *Additive manufacturing of cardiovascular CoCr stents by selective laser melting*, Materials & Design, **119**, 338–350.
9. A. Ziębowicz, A. Woźniak, and B. Ziębowicz, (2018). *The Influence of Technology on the Physicochemical and Electrochemical Properties of the Prosthetic Materials*, Innovations in biomedical engineering. IBE 2017. Eds. Marek Gzik, Ewaryst Tkacz, Zbigniew Paszenda, Ewa Piętka. Cham: Springer International Publishing,, Cham pp. 349–357.
10. L. C. Ardila, F. Garciandia, J. B. González-díaz, P. Álvarez, and A. Echeverria, (2014). Effect of IN718 recycled powder reuse on properties of parts manufactured by means of Selective Laser Melting, Physics Procedia, **56**, 99–107.
11. I. Yadroitsev, A. Gusarov, I. Yadroitsava, and I. Smurov, (2010), *Single track formation in selective laser melting of metal powders*, Journal Materials Processing Technology, **210**(12), 1624–1631.
12. B. Wysocki, P. Maj, A. Krawczyńska, K. Rożniatowska, J. Zdunek, K.J Kurzydłowski, W. Święszkowski, (2017). *Microstructure and mechanical properties investigation of CP titanium processed by selective laser melting (SLM)*, Journal of Materials Processing Technology, **241**, 13–23.
13. M. Król, L. A. Dobrzański, Ł. Reimann, I. Czaja, (2013). *Surface quality in selective laser melting of metal powders*, Archives of Materials Science and Engineering, **60**(2), 87-92.
14. W. E. King, A.T. Anderson, R.M Ferencz, N.E. Hodge, S.A. Khairallah, A.M. Rubenchik, (2015). *Laser powder bed fusion additive manufacturing of metals; physics, computational, and materials challenges*, Applied Physics reviews, **2**(4), 041304.
15. K. C.J. and T. Ch.J., (2011). *High density TI6AL4V via SLM processing: Microstructure and mechanical properties*, Solid Free. Fabr. Proc. an Addit. Manuf. Conf., pp. 475–483.
16. A. Woźniak, M. Adamiak, G. Chladek, and Kasperski, (2019). *The Influence of the Process Parameters on the Microstructure and Properties SLM Processed 316L Stainless Steel*, Archives of Metallurgy and Materials, **65**(1), 73-80.
17. E. Liverani, S. Toschi, L. Ceschini, A. Fortunato, (2017). *Effect of selective laser melting (SLM) process parameters on microstructure and mechanical properties of 316L austenitic stainless steel*, Journal of Materials Processing Technology, **249**, 255–263.
18. B. Zhou, J. Zhou, H. Li, F. Lin, (2018). *A study of the mictrostructure and mechanical properties of Ti6Al4V fabricted by SLM under vacuum*, Materials

Science and Engineering:A, **724**, 1-10.
19. L. Meng., J. Zhao, X. Lan., H. Yang., Z. Wang., (2020). *Multi-objective optimisation of bio-inspired lightweight sandwich structures based on selective laser melting*, Virtual and Physical prototyping, **15**(1), 106-119.
20. Y. He., C. Montgomery, J. Beuth, B. Webler, (2020). *Metlt pool geometry and mictrostructure of Ti6Al4V with B additions processed by selective laser metling additive manufacturing*, Materials and Design, **183**, https://doi.org/10.1016/j.matdes.2019.108126.
21. D. Sun., D. Gu., K. Lin, J. Ma, W. Chen, J. Hugan, X. Sun, M. Chu, (2019). *Selective laser melting of titanium parts: Influence of laser process parameters on macro- and mictrostructures and tensile property*, Powder technology, **342**, 371-379.
22. F. Bartolomeu, M.M. Costa, J.R. Gomes, N. Alves, C.S. Abreu, F.S. Silva, G. Miranda, (2019). *Implant surface design for improved implant stability – A study on Ti6Al4V dense and cellular structure produced by Selective Laser Melting*, Tribology International, **129**, 272-282.
23. D. Gu, Y. Hagedorn, W. Meiners, G. Meng, R.J.S. Batista, K. Wissenbach, R. Poprawe, (2012). *Densifiction behavior, mictrostructure evolution, and wear performance of selective laser melting processed commercially pure titaniu*, Acta Materialia, **60**, 3849-3860.
24. W.H. Kao, Y.L. Su, J.H. Horng, C.Y. Chang, (2018). *Tribological, electrochemical and biocompatibility properties of Ti6Al4V alloy produced by selective laser melting method and then processed using gas nitriding, CN or Ti-C:H coating treatments*, Surface and Coatings Technology, **350**, 172-187.
25. F. Karimzadech, M. Heidarbeigy, A. Saatchi, (2008). *Effect of heat treatment on corosion behavior of Ti-6Al-4V alloy weldments*, Journal of Materials Processing Technology, **206**, 388-394.
26. N.R. Rodrigues, A.C. Alves, F. Toptan, L.A. Rocha, (2018). *Preliminary investigation on the tribocorrosion behaviour of nanotubular structured Ti6Al4V surfaces*, Materials Letters, **213**, 214-217.
27. J. Ju, Y. zhou, K. Wang., Y., Liu., J. Li., M. Kang., J. Wang, (2020). *Tribological investigation of additive manufacturing medical Ti6Al4V alloys against Al_2O_3 ceramic balls in artifical saliva*, Journal of the Mechanical Behavior of Biomedical Materials, **101**, doi: 10.1016/j.jmbbm.2019.103602.

Received: March 17, 2020 / Accepted: December 20, 2020 / Paper available online: December 25, 2020